American Mineralogist, Volume 74, pages 1270–1277, 1989

Barite-celestine intergrowths in Archean plutons: The product of oxidizing hydrothermal activity related to alkaline intrusions

KEIKO HATTORI
Ottawa-Carleton Geoscience Centre, Department of Geology, University of Ottawa, Ottawa, Ontario K1N 6N5, Canada

ABSTRACT

Fine sulfate grains are disseminated within feldspar porphyries of the late Archean Kirkland Lake alkaline igneous complex in the Abitibi greenstone belt. Some grains are completely enclosed within hydrothermal biotite. Bulk compositions of the sulfates are intermediate in the $BaSO_4$-$SrSO_4$ series, the majority containing 15 to 20 mol% $BaSO_4$. Optical properties and the result of acid-etching indicate that they are mechanical mixtures of fine barite and celestine. The consistent bulk chemical compositions, $\delta^{34}S$ values ($\sim +6‰$), and high SO_4^{2-} contents in associated apatite indicate that they were formed as a barian celestine solid solution during oxidizing hydrothermal activity.

Lack of any major thermal events in post-Archean time and low $^{87}Sr/^{86}Sr$ values of sulfates indicate the formation of sulfates in late Archean time. Low metamorphic grade of the area and the occurrence of sulfates within biotites suggest that the sulfate formation was related to the intrusion of the alkaline complex.

INTRODUCTION

Near-surface environments in the Archean are considered to be generally reduced (e.g., Veizer et al., 1982; Walker et al., 1983). Archean sulfate is therefore believed to have been concentrated in (semi-) closed basins by biological oxidation of volcanic sulfide (e.g., Lambert et al., 1978; Reimer, 1980). Findings of barite in many Archean gold veins hosted dominantly by igneous rocks led to the recognition of Archean sulfate of nonbiological origin (Hattori and Cameron, 1986). This paper reports the occurrence of disseminated sulfates in late Archean intrusions at Kirkland Lake in the Abitibi greenstone belt and discusses their origin.

GEOLOGY

The Kirkland Lake area in the Abitibi greenstone belt represents one of the shallowest sections of Archean crust. Clasts of Timiskaming conglomerates, which host the intrusive complex, display evidence of prehnite-pumpellyite facies of regional metamorphism (e.g., Jolly, 1974). The intrusive complex has four major units: augite syenite, felsic syenite, feldspar porphyry, and quartz-feldspar porphyry (Fig. 1). U-Pb zircon ages from a porphyry sample indicate a maximum age of 2680 Ma (T. E. Krogh, personal communication, 1987). The complex is cut by volumetrically minor minette and vogesite dikes, and titanite from the minette dyke provides a minimum age of 2674 ± 2 Ma (Wyman and Kerrich, 1987).

The reader may refer to Jensen and Langford (1985) and Hodgson (1983) for a discussion of regional geology and to Thomson (1950), Ploeger and Crocket (1982), and Hicks and Hattori (1988) for the geology of the mine area and the description of the gold mineralization.

Petrology of the feldspar porphyry unit

Monzodiorite porphyry is the predominant phase in the porphyry unit, and it contains ~25 vol% phenocrysts of (in order of decreasing abundance) plagioclase (3 mm), biotite (1.5 mm), green hornblende (<1 mm), and lesser amounts of magnetite (<0.1 mm), titanite (<0.4 mm), and apatite (<0.2 mm) microphenocrysts. Monzonite porphyry contains ~35 vol% phenocrysts of plagioclase (~3 mm), K-feldspar (~8 mm), biotite (1.5 mm), and minor amounts of green hornblende (1 mm) as well as magnetite (0.1 mm), titanite (<0.3 mm), and apatite (0.2 mm) microphenocrysts. The groundmass of both phases is composed mainly of albite, K-feldspar, and quartz with minor apatite and biotite. Chemical compositions of typical porphyry intrusions are listed in Table 1.

The porphyries, which host most of the gold ore in the camp, have undergone extensive alteration. However, rocks far from gold veins (>100 m), obtained mainly from the drill cores, are olive black (GSA color code: 5Y2/1) to dark grey (N3) and exhibit preserved minerals and textures that predate the alteration related to the gold mineralization. Foliation, veinlets, and fractures are virtually absent from the samples. Only the least-altered rock samples contain the sulfates described in this report.

Alteration observed in the least-altered samples includes formation of hematite and titanite on rims of magnetite, formation of fine-grained K-feldspar and albite on the margin of feldspar grains, partial recrystallization of groundmass feldspars, dissemination of minor ankerite in groundmass and the formation of secondary biotite (Hicks and Hattori, 1988).

Secondary biotite commonly replaces hornblende and primary biotite and overgrows the primary biotite. It is

0003–004X/89/1112–1270$02.00

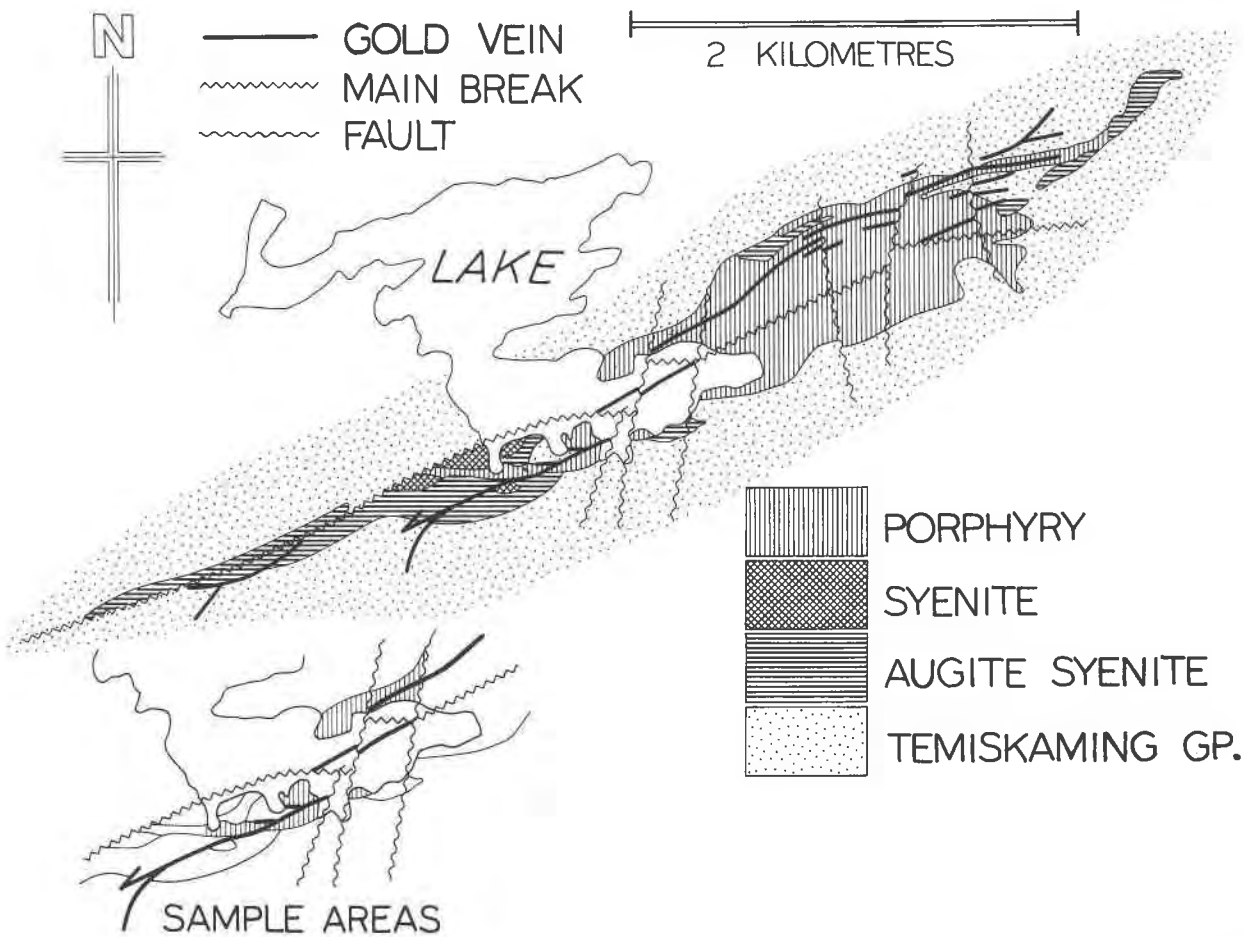

Fig. 1. Geologic map of the Kirkland Lake area. The studied samples were collected from the area indicated in the inserted map. Modified after Ploeger and Crocket (1982).

characterized by its light color and high Mg (X_{phl}^{biot} = ~70 mol%; Fig. 2). Chemical compositions of secondary biotite vary within a section, and coarse one in the groundmass is greenish and rich in F (<1.8 wt%) and BaO (<2.8 wt%; Table 2).

Occurrence of sulfates

Sulfates are found as common accessory minerals in various phases of the porphyry collected in this study (Fig. 1). Sulfates occur disseminated within secondary biotite (Figs. 3 and 4), in the margins of albite and K-feldspar phenocrysts, and within the groundmass. Sulfate grains in biotite are commonly rectangular (1:2; Fig. 3), and some are elongated with aspect ratios up to 10:1 along the cleavage planes of biotite (Fig. 4). Grains in the groundmass are mostly anhedral and range in size from less than 2 to 20 μm, but a single grain of ~100 μm in length has been observed. Some grains in the groundmass enclose one or two minute grains of apatite, albite, and K-feldspar. An apatite inclusion in sulfate contains 0.9 wt% SO_3 (Table 3), which is higher than the SO_3 contents in microphenocryst apatite. High SO_3 contents in apatite (Table 3) indicate an SO_4-rich fluid during formation.

Sulfate grains are transparent under the microscope and have relatively high refractive indices and very low birefringence, $\delta < 0.006$, similar to those of apatite. There is no cleavage observed in the grains, although cleavage of {001} would be expected in a sulfate (Deer et al., 1963). They also show incomplete or undulatory extinction (Fig. 3c). Elongated sulfate grains in biotite do not show parallel extinction (Fig. 3b). The extinction under crossed polarizers is attained at an oblique angle (20° to 27°; Fig. 3c). These optical properties are not consistent with those of a single sulfate phase.

Chemical composition of sulfates

More than 40 analyzed grains of sulfate show only peaks of Ba, Sr, and S in the energy-dispersive spectra. Other cations, including Ca and Pb, are below detection limits (<0.3 wt%). Semiquantitative analyses show that most grains have similar chemical compositions; Ba/(Ba + Sr) molar ratios all fall in the range of ~0.15 to 0.20 (Table

Table 1. Chemical compositions of typical porphyry intrusions containing barium and strontium sulfates

Sample number	KDH83	KH414-12	KDH135
SiO_2 (wt%)	64.12	61.41	62.27
TiO_2 (wt%)	0.32	0.41	0.39
Al_2O_3 (wt%)	14.55	14.22	14.64
FeO* (wt%)	1.72	2.40	1.94
Fe_2O_3 (wt%)	1.44	1.47	1.95
MgO (wt%)	1.70	3.08	2.01
CaO (wt%)	2.70	3.33	3.28
Na_2O (wt%)	5.22	4.38	5.66
K_2O (wt%)	2.90	3.38	2.49
P_2O_5 (wt%)	0.21	0.36	0.27
MnO (wt%)	0.06	0.07	0.07
S (wt%)	0.11	0.07	0.16
Ba** (ppm)	3531	3047	3169
Cr (ppm)	116	167	103
Zr (ppm)	260	217	256
Sr (ppm)	5666	2334	5934
Rb** (ppm)	73	115	66
Y (ppm)	16	17	14
Zn (ppm)	59	61	52
Ni (ppm)	14	58	16
V (ppm)	45	64	72
Sc** (ppm)	6.8	9.1	8.8
Cs** (ppm)	2.8	9.3	2.8
La** (ppm)	36	52	45
Ce** (ppm)	75	110	95
Nd** (ppm)	36	52	45
Sm** (ppm)	6.4	8.4	7.8
Eu** (ppm)	1.57	1.99	1.87
Tb** (ppm)	0.61	0.74	0.79
Dy** (ppm)	3.0	3.8	3.6
Ho** (ppm)	0.66	0.78	0.84
Yb** (ppm)	1.54	1.60	1.62
Lu** (ppm)	0.20	0.23	0.23
Total (wt%)	96.15	95.58	96.29

Note: KDH83—Biotite monzodiorite porphyry, DDH 24 from 800-ft (~244-m) level at the Lake Shore property, 143–145 ft (~44 m) deep. KH414-12—Biotite monzodiorite porphyry, DDH 15 from 1500-ft (~457-m) level at the Lake Shore mine, 227 ft (~69 m) deep. KDH135—Hornblende-biotite monzodiorite porphyry, DDH 68 from 1000-ft (~300-m) level at the Lake Shore mine, 58 ft (~18 m) deep.

* Determined by titration technique.

** Determined by INAA at Ecole Polytechnique. All elements were determined by XRF, except as noted.

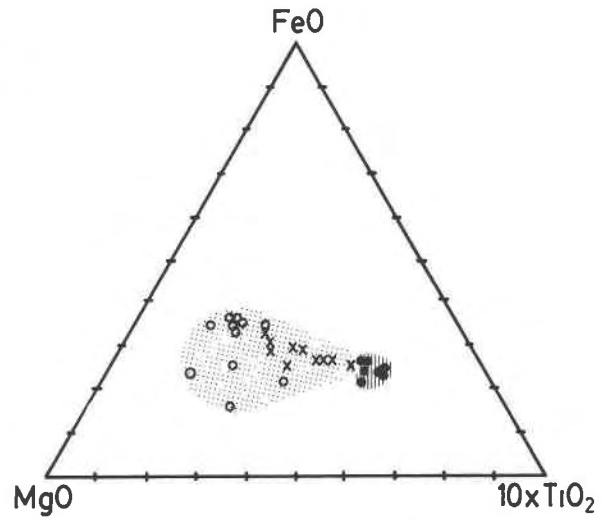

Fig. 2. Triangular diagram showing the composition of biotite, in terms of molecular FeO, MgO, and TiO_2; total Fe expressed as FeO. Solid circles = primary biotite; crosses = brown secondary biotite; open circles = green secondary biotite. Striped area = field of the compositions of primary biotite; dotted area = field of the compositions of secondary biotite.

4; X-ray maps of Sr$L\alpha$ and Ba$L\alpha$ in Figs. 4b, 4c, 5a, and 5b).

Intragrain compositional variations were examined by electron microprobe and SEM. Backscattered-electron images and X-ray maps of Sr$L\alpha$ and Ba$L\alpha$ at 3000× to 4000× magnification (Figs. 4b, 4c, 5a, and 5b) do not reveal exsolution textures nor apparent inhomogeneity. Other grains, however, show patterns with slightly brighter and darker spots in backscattered-electron images corresponding to Ba- and Sr-rich domains (Table 4). Because celestine is far more soluble than barite at room temperature, samples were acid-etched (1:5 HCl) and specimens were examined by SEM; the solution was examined for its Sr and Ba contents by flame AAS. In two specimens, pure tabular barite was found in cavities that were once filled with sulfates (Fig. 6b). In most cases, blades of sulfates containing Ba and Sr remain in the sites (Fig. 6a), but the solution contained predominantly Sr. Further etching of the samples removed sulfates completely. The results indicate that some sulfate grains are made up of coarser barite and celestine (~1 μm), but most are mixtures of much finer grains of the two sulfates. Because celestine is the major sulfate in the mixture, dissolution of celestine caused disintegration of grains and removal of sulfates from the sample.

Isotopic compositions of sulfates

S-isotope values of the sulfate are in a narrow range from +6 to +7‰ (Table 5b). The values are much larger than the values of sulfides in veins in the area; $\delta^{34}S$ values of sulfides in the auriferous veins range from −16 to −6‰ (Cameron and Hattori, 1987, and Table 5b), and the values in disseminated pyrite near the veins also are similarly low (Table 5b).

Sr was extracted by cold NaCl solution and the Sr-isotope compositions were determined. The values are low (0.7027 and 0.7040; Table 6).

Discussion

There are three possible modes of origin of the sulfates in the samples: (1) a primary magmatic origin in which the sulfates crystallized from the melt, (2) a magmatic-hydrothermal origin, or (3) a supergene origin.

S-isotope data do not support the possibility of a supergene origin by oxidation of sulfides. Such sulfate would have low $\delta^{34}S$ values similar to the source sulfide, as sulfides in the area have low $\delta^{34}S$ (Table 5b). Instead, the observed values of $\delta^{34}S$ are similar to those for magmatic anhydrite (+6.5 to 9.5‰; Arculus et al., 1983; Rye et al., 1984) and those for early-formed sulfate in the biotite-alteration zone in porphyry copper deposits, (+7.3 to 9.7‰; Field and Gustafson, 1976; +6.6 to +8.1‰; Shelton and Rye, 1982).

TABLE 2. Compositions of secondary biotite associated with sulfates

	RT31-F	880427-10
SiO_2	37.14	38.89
TiO_2	3.43	1.18
Al_2O_3	13.87	14.27
Cr_2O_3	n.d.	0.39
MgO	15.36	17.88
MnO	0.13	n.d.
FeO*	14.67	14.92
Na_2O	0.13	0.06
K_2O	8.96	9.35
CaO	n.d.	n.d.
BaO	1.38	0.21
F	n.d.	1.58
Cl	n.d.	n.d.
$-O \equiv F$	0.00	0.67
Total	95.07	98.06
Cations calculated on the basis of 11 oxygen equivalents		
Si^{4+}	2.806	2.796
Al^{3+}	1.194	1.204
T site	4.000	4.000
Al^{3+}	0.041	0.005
Mg^{2+}	1.730	1.917
Mn^{2+}	0.008	0.000
Fe^{2+*}	0.927	0.897
Cr^{3+}	0.000	0.022
Ti^{4+}	0.195	0.064
M site	2.901	2.895
Na^+	0.019	0.008
K^+	0.863	0.858
Ca^{2+}	0.000	0.000
Ba^{2+}	0.041	0.006
A site	0.927	0.872
F^-	0.000	0.359
Cl	0.000	0.000
O^{2-}	11.000	10.641

Note: n.d., below the detection limit (<0.02 wt%).
* Total Fe is calculated as FeO.

Consistent bulk chemical compositions of the sulfates in the series $BaSO_4$-$SrSO_4$ also support this view. Because there is immiscibility in the series at temperatures below 100 °C (Malinin and Urusov, 1983), sulfates formed in supergene conditions would not have intermediate compositions. Their occurrence within biotite and the lack of sulfate veinlets in the samples are also consistent with their formation at high temperatures.

Sulfates may be formed as a primary phase in magmas whose f_{O_2} is near the NNO buffer (Carroll and Rutherford, 1987). The magmas from which the Kirkland Lake porphyries were formed were apparently oxidized, as indicated by early formation of titanite and magnetite together with hornblende (Noyes et al., 1983) and high Mg/Fe values in the primary biotite (Fig. 2; Chivas, 1981). However, the occurrence of sulfates in secondary biotites and the variation in Sr in the porphyry samples, >4000 ppm in sulfate-bearing samples (Table 1) and ~1000 ppm in

TABLE 3. Chemical compositions of apatite (in wt%)

	A	B	C
CaO	54.74	54.20	55.91
FeO	n.d.	n.d.	—
SrO	n.d.	n.d.	n.d.
P_2O_5	42.04	41.35	41.61
SO_3	0.24	0.39	0.90
Cl	n.d.	n.d.	—
Total	97.02	95.94	98.42

Note: n.d., not detected; —, not determined. (A) Apatite microphenocrysts in sample KDH136 (DDH 93 from 1000-ft (~300-m) level, 6–7 ft (~2 m) deep at the Lake Shore property). (B) Apatite microphenocrysts in sample KH414-12. (C) Apatite enclosed in the sulfate grains in groundmass.

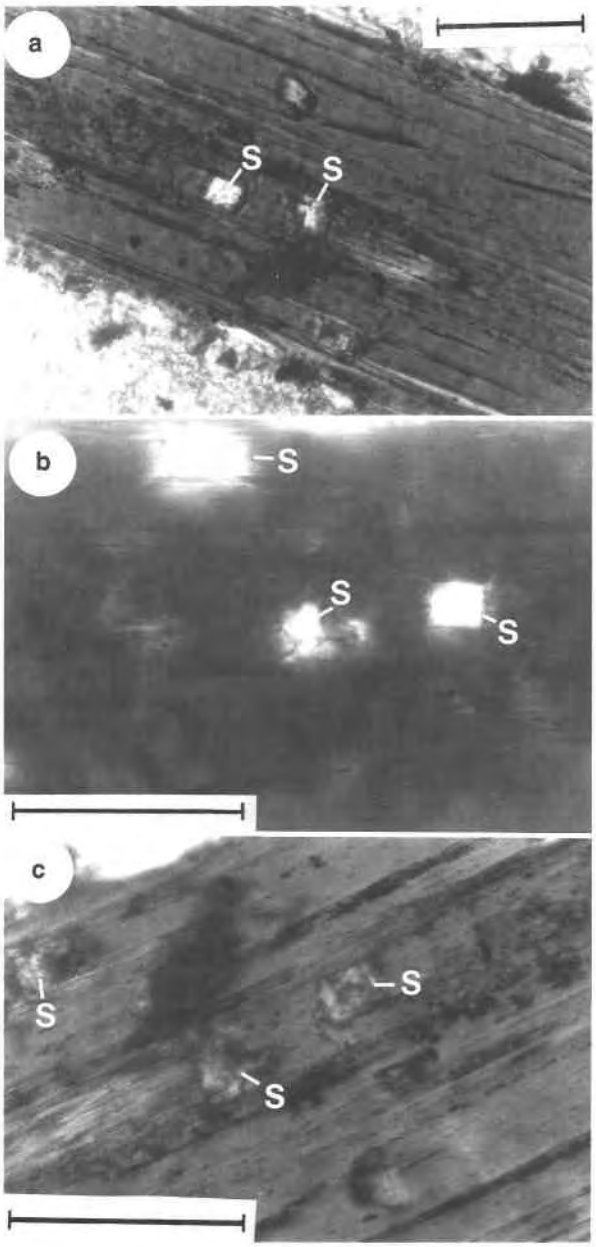

Fig. 3. Photomicrograph showing typical occurrence of sulfates within biotite (sample no. KDH83). (**a**) Plane-polarized light; (**b**) and (**c**) cross-polarized light. Scale bar is equivalent to 100 μm. Note that the sulfate grains (marked S) do not show parallel extinction (b) and their extinction is incomplete (c).

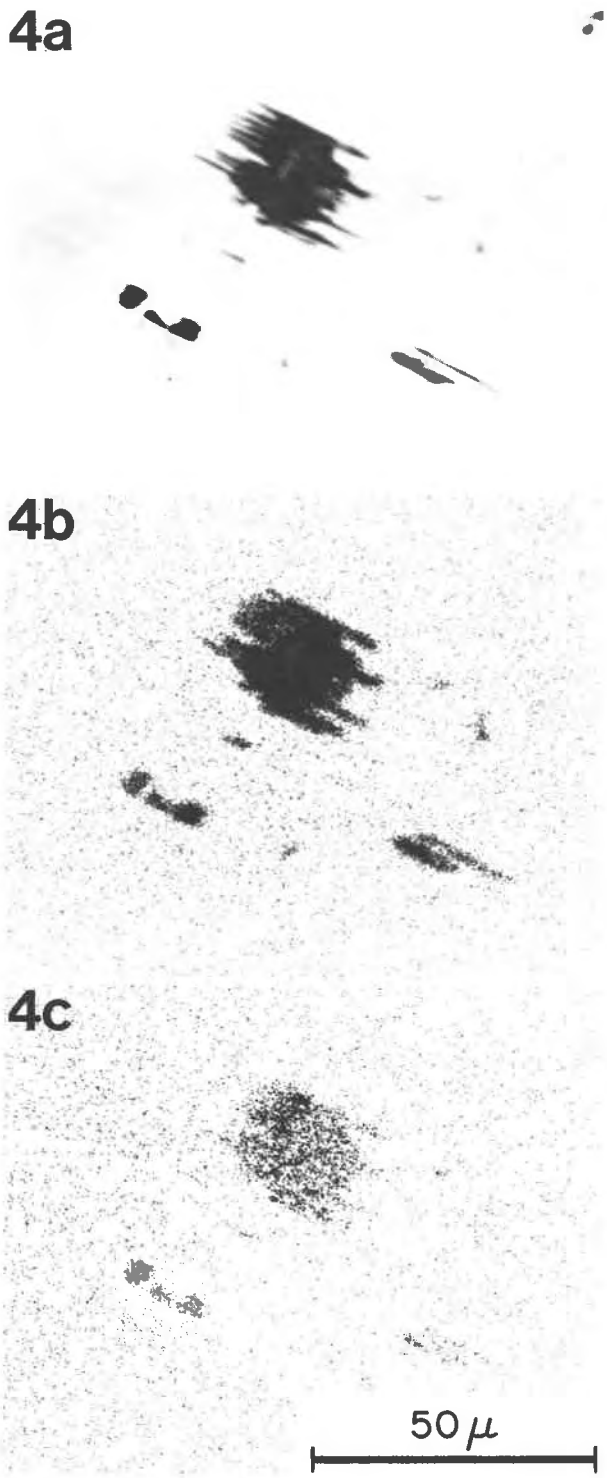

Fig. 4. (a) Backscattered-electron image, (b) Sr$L\alpha$ X-ray map, and (c) Ba$L\alpha$ X-ray map of sulfate grains within biotite shown in Fig. 3.

Table 4. Chemical compositions of sulfates (electron-microprobe analysis)

	A	B	C	D
SrO (wt%)	41.9	45.0	43.7	50.9
BaO (wt%)	16.9	13.3	14.8	6.4
CaO (wt%)			0.1	0.3
SO_3 (wt%)	41.2	41.7	41.5	42.7
$SrSO_4$ (mol%)	78.6	83.35	81.14	91.30
$BaSO_4$ (mol%)	21.4	16.65	18.59	7.77
$CaSO_4$ (mol%)			0.26	0.96

Note: (A) Grains within secondary biotite (sample KDH83). (B) Darkest spot of the grain that showed inhomogeneity in backscattered-electron image (sample KDH84). (C) Brightest spot of the same grain as B (sample KDH84). (D) Sr-rich grain in the groundmass (sample KDH135).

sulfate-free samples, suggest a hydrothermal origin of the sulfates.

Biotite is a common metamorphic mineral. However, the biotite in the Kirkland Lake intrusive complex is not a product of regional metamorphism because of low regional metamorphic grade (e.g., Jolly, 1974). The formation of sulfates in the intrusions is, therefore, related to the emplacement of intrusive complex. Low $^{87}Sr/^{86}Sr$ ratios in the sulfates support this view. Because the porphyry unit contains a significant amount of Rb (70 to 300 ppm), any sulfate formed in post-Archean time would be rich in radiogenic ^{87}Sr.

Decompression of magmas during their ascent allows a release of volatiles. SO_2 is the principal S-bearing species in the volatile phase of oxidized magmas, and it forms SO_4^{2-} through a hydrolysis reaction. The release of volatiles from the studied porphyries is supported by the presence of miarolitic cavities (Hicks and Hattori, 1988) and titanization and hematitization along cracks and margins of magnetite microphenocrysts.

Sulfates display retrograde solubilities at various temperature ranges. Solubilities of celestine are retrograde at temperatures below ~400 °C (Strubel, 1966). Solubilities of barite in dilute solutions, $<1m$ NaCl, are retrograde at temperatures higher than 100 °C (Blount, 1977). Retrograde solubilities of barite are also reported in saline fluids at temperatures between 350 and 450 °C (Strubel, 1967). The occurrence of the mixture of celestine and barite in the groundmass of the studied samples may suggest that the pervasive hydrothermal activity ceased at temperatures higher than 400 °C. Lack of retrograde alteration of biotites may support this interpretation.

Anhydrite is the most common sulfate in igneous rocks either as phenocrysts or alteration product. The lack of anhydrite in studied samples may be attributed to low Ca/Sr and Ca/Ba ratios of the host intrusions (Table 1) and high CO_2 of fluid responsible for the formation. Solubilities of anhydrite are over an order of magnitude larger than those of celestine and barite in a solution of a given salinity (Strubel, 1966, 1967; Blount and Dickson, 1969), which suggests that precipitation of anhydrite requires approximately the concentration of Ca^{2+} to be ten

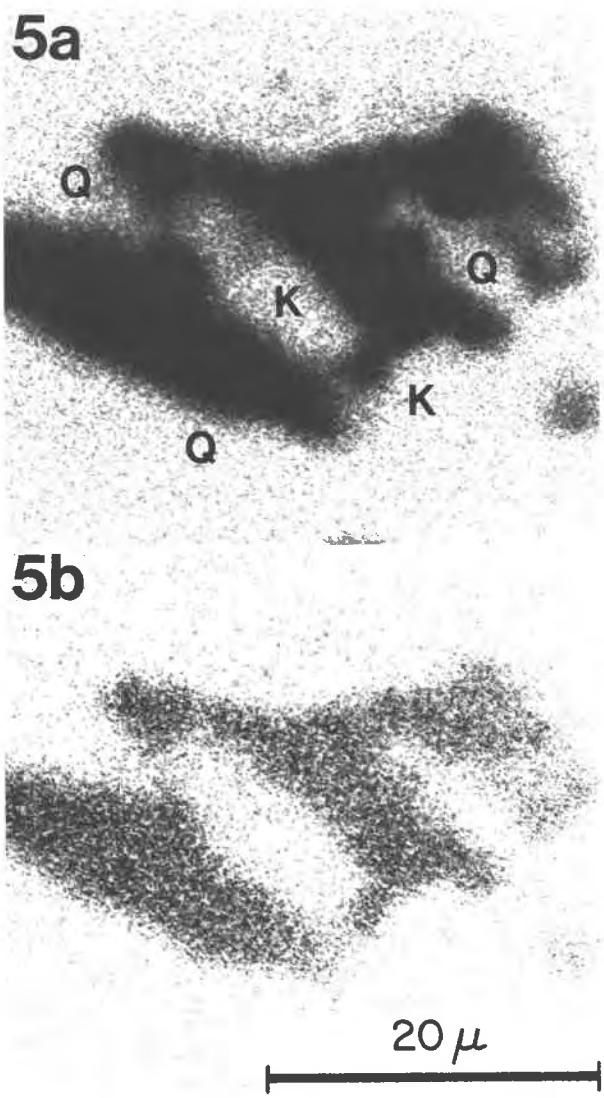

Fig. 5. (**a**) Sr$L\alpha$ X-ray map and (**b**) Ba$L\alpha$ X-ray map of sulfate in groundmass. Q = quartz, K = K-feldspar.

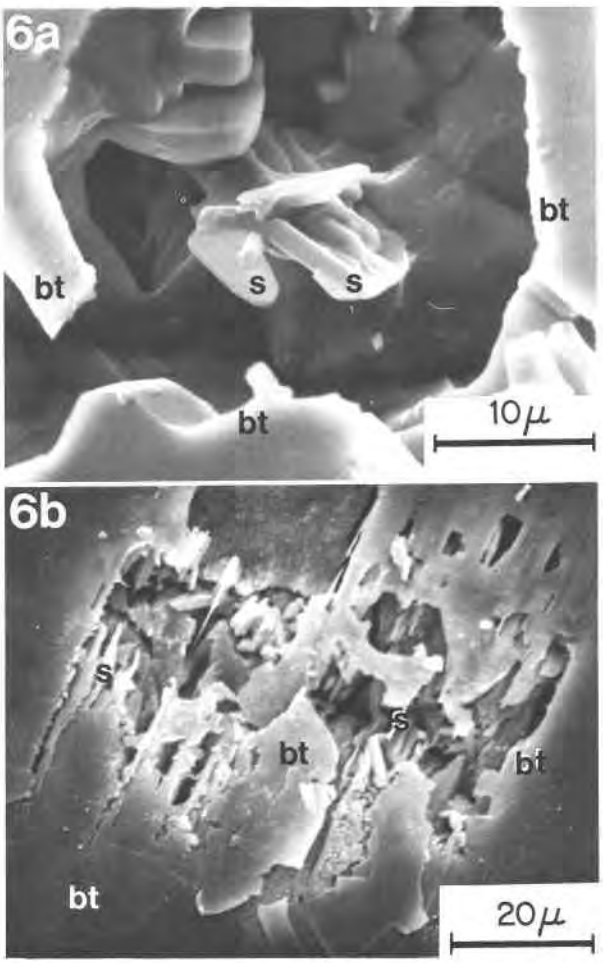

Fig. 6. Scanning-electron-microscope image of sulfate after etching with acid. (**a**) Tabular barite crystals (s) in biotite (bt) (sample RT-39). (**b**) Sulfate blades (s) containing Sr and Ba in biotite (bt). Photomicrographs of the grain shown in Figs. 3 and 4 after acid etching.

times larger than Sr^{2+}. The host porphyry rocks are rich in Sr and Ba, but low in Ca (Ca/Sr molar ratios, 7 to 8). Furthermore, K-feldspar in the Kirkland Lake intrusive complex is rich in BaO (<3.01 wt%) and SrO (<2.88 wt%). Recrystallization of feldspars during hydrothermal activity would have released Ba^{2+} and Sr^{2+} to the fluids. Finally, fluids were rich in CO_2, indicated by minor but ubiquitous occurrences of ankerite in the groundmass. Ca^{2+} concentration of such fluids would have been buffered by carbonate, which would have prevented the formation of anhydrite.

Table 5a. S-isotope compositions of sulfates

Sample	Total S (wt%)	$\delta^{34}S_{CDT}$ (‰)
KDH82	0.11	+6.2
KDH119	0.08	+6.2
KDH130	0.09	+6.7
KH414-12	0.07	+7.0
RT32	0.12	+6.0
		+6.1*

* Acid leaching of sulfates (see App. 1).

Table 5b. S-isotope compositions of sulfides

Sample	Description	$\delta^{34}S_{CDT}$ (‰)
KH85022-04	North vein	−11.7
KH860220-31	Syenite, 0.5 m from vein	−10.8
KH850220-60	Network vein in porphyry	−3.3
KH850220-71	Dissemination of pyrite in porphyry	−9.6
KH860529-09	Pyrite in porphyry, 0.3 m from South vein	−9.4
KH860529-10	Pyrite in South vein	−10.4
KH880427-16	Molybdenite-rich part of the main vein	−9.1
KH880427-15	Pyrite cubes in fault gouge near the North vein	−6.7
RT-05	Sericitized-pyritized wallrock	−10.3
RT-12	Hematitized wallrock	−2.8

TABLE 6. Sr-isotope compositions of sulfate

Sample	$^{87}Sr/^{86}Sr$
KDH83	0.70271 ± 0.00002
KDH119	0.70403 ± 0.00006

The occurrence of the primary sulfate minerals has been recognized within only historic lavas (e.g., Arculus et al., 1983; Luhr et al., 1984). The absence of anhydrite phenocrysts in prehistoric igneous rocks is attributed to weathering because of the high solubility of sulfate (Arculus et al., 1983). Similarly, magmatic-hydrothermal sulfates are common in Phanerozoic intrusions, but their occurrence in Archean terranes is very limited. This is partly due to erosion of the upper section of Archean crust and partly due to the retrograde solubilities of many sulfates. Most magmatic and magmatic-hydrothermal sulfates would have been dissolved during the waning stage and/or later hydrothermal activity.

In Phanerozoic porphyry deposits, dissolution of earlier formed magmatic-hydrothermal sulfates affected the chemistry of subsequent hydrothermal fluids and resulted in redistribution of metallic minerals (e.g., Shelton and Rye, 1982). Under the generally reducing Archean conditions, the dissolution of sulfate would have had a profound effect on the chemistry of subsequent hydrothermal fluids at <400 °C by raising their f_{O_2} to that of the H_2S-SO_4^{2-} buffer. Increase in oxidation of fluids to the H_2S-SO_4^{2-} buffer during the waning stage of hydrothermal activity would result in transport of only selected elements, because most metals are less soluble in more oxidized fluids and at lower temperatures. Au and Mo belong to this group of elements that could be concentrated by oxidized fluids.

SUMMARY

1. Physically mixed grains of barite-celestine occur disseminated in the least-altered monzonitic porphyry intrusions of Archean age at Kirkland Lake, Ontario.

2. The occurrence of sulfates within secondary biotite, bulk Ba/Sr ratios and $\delta^{34}S$ and $^{87}Sr/^{86}Sr$ ratios of the sulfates indicate that they were most likely formed at high temperatures, >400 °C, as an intermediate-composition member in the $BaSO_4$-$SrSO_4$ series during the emplacement of the alkaline complex in late Archean time.

Many epizonal intrusions of Archean age should be carefully studied to identify the occurrence of sulfate as it may be more common than is generally realized.

ACKNOWLEDGMENTS

I thank F. Ploeger and G. Hemcsok of Lac Minerals and L. Cunningham for their help in sample collection, T. S. Ercit of the National Museum of Natural Sciences for access to the electron microprobe, T. Wrzesniewska for her help at the SEM laboratory, N. Mrorriset for the extraction of S, R. Theriault for Sr-isotope analysis, K. Sears for XRF and Fe^{2+} analyses, and G. Kennedy for the INAA work. Some samples were collected by R. Theriault and K. Hicks. This project was funded by an Ontario Geoscience Research Grant (no. 313) and by the Natural Sciences and Engineering Research Council of Canada (no. AO616). Comments on earlier versions of the manuscript by R. Martin of McGill University, P. Roeder of Queen's University, M. J. Rutherford of Brown University, G. K. Czamanske of the U.S. Geological Survey, A. C. Colvine and M. E. Cherry of the Ontario Geological Survey, and T. S. Ercit of the National Museum of Natural Sciences are also appreciated.

REFERENCES CITED

Arculus, R.J., Johnson, R.W., Chappell, B.W., McKee, C.O., and Sakai, H. (1983) Ophiolite-contaminated andesites, trachybasalts, and cognate inclusions of Mount Lamington, Papua New Guinea: Anhydrite-amphibole–bearing lavas and the 1951 cumulodome. Journal of Volcanology and Geothermal Research, 18, 215–247.

Blount, C.W. (1977) Barite solubilities and thermodynamic quantities up to 300° C and 1400 bars. American Mineralogist, 62, 942–957.

Blount, C.W., and Dickson, F.W. (1969) Solubility of anhydrite ($CaSO_4$) in NaCl-H_2O from 100° to 450°C and 1 to 1000 bars. Geochimica et Cosmochimica Acta, 33, 227–245.

Carroll, M.R., and Rutherford, M.J. (1987) The stability of igneous anhydrite: Experimental results and implications for sulfur behaviour in the 1982 El Chichon trachyandesite and other evolved magmas. Journal of Petrology, 28, 781–801.

Cameron, E.M., and Hattori, K. (1987) Archean gold mineralization and oxidized hydrothermal fluids. Economic Geology, 82, 1177–1191.

Chivas, A.R. (1981) Geochemical evidence for magmatic fluids in porphyry copper mineralization. Contribution to Mineralogy and Petrology, 78, 389–403.

Deer, W.A., Howie, R.A., and Zussman, J. (1963) Rock-forming minerals, vol. 5, Non-silicates, 371 p. Longmans, Green, London.

Field, C.W., and Gustafson, L.B. (1976) Sulfur isotopes in the porphyry copper deposits at El Salvador, Chile. Economic Geology, 71, 1553–1548.

Hattori, K., and Cameron, E.M. (1986) Archaean magmatic sulphate. Nature, 319, 45–47.

Hicks, K.D., and Hattori, K. (1988) Magmatic-hydrothermal and wall-rock alteration petrology at the Lake Shore gold deposit, Kirkland Lake, Ontario. Ontario Geological Survey Miscellaneous Paper 140, 192–204.

Hodgson, C.J. (1983) Preliminary report on the Timmins–Kirkland Lake area. Ontario Geological Survey Open File Report 5467, 197 p.

Jensen, L.S., and Langford, F.F. (1985) Geology and petrogenesis of the Archean Abitibi belt in the Kirkland Lake area, Ontario. Ontario Geological Survey Miscellaneous Paper 123, 130 p.

Jolly, W.T. (1974) Regional metamorphic zonation as an aid in the study of Archean terrains, Abitibi region, Ontario. Canadian Mineralogist, 12, 499–508.

Lambert, I.B., Donnelly, T.H., Dunlop, J.S.R., and Groves, D.I. (1978) Stable isotopic compositions of early Archaean sulphate deposits sulphate deposits of probably evaporitic and volcanogenic origins. Nature, 276, 808–811.

Luhr, J.F., Carmichael, I.S.E., and Varekamp, J.C. (1984) The 1982 eruptions of El Chichon volcano, Chiapas, Mexico: Mineralogy and petrology of the anhydrite-bearing pumices. Journal of Volcanology and Geothermal Research, 23, 69–108.

Malinin, S.D., and Urusov, V.S. (1983) The experimental and theoretical data on isomorphism in the $(Ba,Sr)SO_4$ system in relation to barite formation. Geochemistry International, 20, no. 5, 70–80.

Noyes, H.J., Wones, D.R., and Frey, F.A. (1983) A tale of two plutons: Petrographic and mineralogic constraints on the petrogenesis of the Red Lake and Eagle Lake plutons, central Sierra Nevada, California. Journal of Geology, 91, 353–379.

Ploeger, F.R., and Crocket, J.H. (1982) Relationship of gold to syenitic intrusive rocks in Kirkland Lake. In R.W. Hodder et al., Eds., Geology of Canadian gold deposits, Proceedings of the CIM gold symposium. Canadian Institute of Mining and Metallurgy Special Volume 24, 9–14.

Reimer, T.O. (1980) Archean sedimentary baryte deposits of the Swaziland supergroup (Barberton Mountain Land, South Africa). Precambrian Research, 12, 393–410.

Rye, R.O., Luhr, J.F., and Wasserman, M.D. (1984) Sulfur and oxygen

isotopic systematics of the 1982 eruptions of El Chichon volcano, Chiapas, Mexico. Journal of Volcanology and Geothermal Research, 23, 109–123.

Sasaki, A., Arikawa, Y., and Folinsbee, R.E. (1979) Kiba reagent method of sulfur extraction applied to isotopic work. Bulletin of Geological Survey of Japan, 30, 241–245.

Shelton, K.L., and Rye, D.M. (1982) Sulfur isotopic compositions of ores from Mines Gaspé, Quebec; An example of sulfate-sulfide isotopic disequilibria in ore-forming fluids with applications to other porphyry-type deposits. Economic Geology, 77, 1688–1709.

Strubel, G. (1966) Die hydrothermale Löslichkeit von Cölestin im System $SrSO_4$-NaCl-H_2O. Neues Jahrbuch für Mineralogie Monatshefte, 99–108.

——— (1967) Zur Kenntnis und genetischen Beduetung des Systems $BaSO_4$-NaCl-H_2O. Neues Jahrbuch für Mineralogie Monatshefte, 223–233.

Thomson, J.E. (1950) Geology of Teck Township and the Kenogami Lake area, Kirkland Lake gold belt. Ontario Department of Mines Annual Report, 57, Part 5, 1–53.

Veizer, J., Compston, W., Hoefs, J., and Nielsen, H. (1982) Mantle buffering of the early oceans. Die Naturwissenschaften, 69, 173–180.

Walker, J.C.G., Klein, C., Schidlowski, M., Schopf, J.W., Stevenson, D.J., and Walter, M.R. (1983) Environmental evolution of the Archean–early Proterozoic Earth. In J. W. Schopf, Ed., Earth's earliest biosphere, p. 260–290. Princeton University Press, Princeton, New Jersey.

Wyman, D.A., and Kerrich, R. (1987) Archean lamprophyres I: Distribution and tectonic setting. Geological Association of Canada–Mineralogical Association of Canada, Programme and Abstracts, 12, 102.

Manuscript received October 27, 1988
Manuscript accepted July 10, 1989

Appendix 1. Analytical methods

Major- and trace-element contents of whole-rock samples were determined by XRF on samples fused with a Li_2CO_3-$Li_2B_4O_7$ mixture. Fe^{2+} contents were determined by a standard titration technique. Chemical analyses of minerals were carried out using a JEOL-733 electron microprobe equipped with a Tracor Northern 5500 energy-dispersive spectrometer and Tracor Northern 5600 automation. For all samples, the general operating conditions were as follows: 15-kV accelerating voltage, 25-nA beam current, 50-s count time (or 0.5% precision, whichever was achieved first). For the apatites and biotites, data reduction was carried out on data collected with wavelength spectrometers using the Tracor-Northern 5600 program TASK; standards were apatite (P, Ca) and anhydrite (S) for apatites, chlorite (Al, Si, Mg), biotite (Fe, Ti, K), diopside (Ca), chromite (Cr), albite (Na), willemite (Mn), tugtupite (Cl), sanbornite (Ba), and fluorellestadite (F) for biotite analysis. In the case of sulfates, compositions could only be determined semiquantitatively because of the small grain size (generally less than 10 μm) and the decomposition of the samples under high beam current. For this purpose, the semiquantitative program SSQ in the Tracor-Northern 5500 was used for the analysis of the energy-dispersive spectra of the minerals. Ca contents were calculated using wavelength-spectrometer data in conjunction with the TASK program. SEM study was carried out using SEMCO Nanolab 7 attached KEVEX energy-dispersive X-ray analyzer. The accelerating voltage of the beam was set at 15-kV throughout the analysis.

For isotope analysis, S in the samples was extracted by "Kiba-reagent" (Sasaki et al., 1979). Because no sulfides were observed in sections under microscope, the values of total S are considered to be those for sulfates. To ensure the result, sulfate S was leached from several samples by 5% HCl solution and then precipitated as $BaSO_4$. SO_2 for isotope analysis was extracted from the $BaSO_4$ by mixing with Cu_2O and SiO_2 and combusting the mixture at 1000 °C. The isotopic compositions were obtained using VG micromass 602E, and the data are expressed with respect to the Canon Diablo meteorite standard using the familiar δ notation. Overall analytical precision is ± 0.1‰.

Sr was extracted from the rock powder (less than 2 μm) by constantly stirred cold 2*N* NaCl solution for 2 d, which prevented dissolution of Sr from carbonates and silicate minerals. Sr was then separated from the NaCl solution using a cation-exchange resin and then analyzed by mass spectrometry on a Finnigan Mat 261.